

Cite this: DOI: 00.0000/xxxxxxxxxx

Directional Clogging and Phase Separation for Disk Flow Through Periodic and Diluted Obstacle Arrays

C. Reichhardt and C. J. O. Reichhardt

Received Date
Accepted Date

DOI: 00.0000/xxxxxxxxxx

We model collective disk flow through a square array of obstacles as the flow direction is changed relative to the symmetry directions of the array. At lower disk densities there is no clogging for any driving direction, but as the disk density increases, the average disk velocity decreases and develops a drive angle dependence. For certain driving angles, the flow is reduced or drops to zero when the system forms a heterogeneous clogged state consisting of high density clogged regions coexisting with empty regions. The clogged states are fragile and can be unclogged by changing the driving angle. For large obstacle sizes, we find a uniform clogged state that is distinct from the collective clogging regime. Within the clogged phases, depinning transitions can occur as a function of increasing driving force, with strongly intermittent motion appearing just above the depinning threshold. The clogging is robust against the random removal or dilution of the obstacle sites, and the disks are able to form system-spanning clogged clusters even under increasing dilution. If the dilution becomes too large, however, the clogging behavior is lost.

There are a variety of systems that can be described as a loose assembly of particles which exhibit jamming behaviors. At lower densities, flow occurs easily in such systems, but at high densities the system can act like a solid in which all flow ceases^{1–6}. Jamming has been extensively studied as a function of density^{1,3}, shear⁶, particle shape^{5,7–9}, and friction effects^{10,11}. Many of these studies involved no quenched disorder so that the system can be described as containing only particle-particle interactions. It is also possible for the particle motion to be stopped by some form of external constraints, such as flow through bottlenecks or funnels^{12–17}, motion through a mesh^{18–22}, flow over a disordered substrate^{23–25}, or flow in porous media^{26–32}. The particle flow stops when the combination of the particle density and the obstacle density is high enough. Open questions include whether the cessation of flow in systems with quenched disorder is best described as jamming or clogging, as well as how to distinguish between these two phenomena.

There are several limiting cases for jamming and clogging behavior. For example, frictionless disks have a well defined jamming density ϕ_j in the absence of obstacles. If a small number of obstacles are added, the system can still be described as reaching a jamming point at a slightly lower density $\phi < \phi_j$ due to the diverging length scale l_j that emerges as the jamming density in the clean system is approached. Jamming, which is associated with a uniform particle density throughout the system, occurs once the average distance between obstacles l_{obs} becomes smaller than the

jamming length scale, $l_{\text{obs}} < l_j$. Another limit is the clogging of a single particle, which can arise for flow along the x direction through a square array of obstacles when the obstacle radius becomes large enough that the particle cannot fit in the space between adjacent obstacles. Between the jamming and single particle clogging limits, a variety of other types of collective clogging behaviors are possible in which groups of particles come together to create a locally stuck region.

Several studies addressing the effects of a small number of obstacles or weak quenched disorder on the jamming transition show that the jamming density decreases as obstacles are added^{33–35}, while other studies have focused on a crossover from jamming to clogging behavior for particles moving through obstacle arrays^{36–39}. Péter *et al.*³⁷ considered an assembly of monodisperse particles moving over a random obstacle array. For a small number of obstacles, they found jamming behavior in which the particle density is uniform in the motionless state. Once the obstacle density exceeds a certain threshold, the system exhibits a clogged state down to very low particle densities. The clogged state is highly heterogeneous and contains local patches in which the particle density is close to the jamming density along with other patches in which there are few or no particles. Additionally, the system requires time in which to gradually organize into a particular clogged configuration, whereas the jammed states form very rapidly. Nguyen *et al.*³⁶ studied an assembly of bidisperse grains moving through a two-dimensional periodic obstacle array and also found a transition to a clogged state characterized by the formation of a high density phase coexisting with a low

density phase. In this case, the susceptibility to the formation of a clogged state depended on the direction of the flow relative to the substrate symmetry directions. For example, when the obstacles are small, the system does not jam when driven along the x -direction, but for driving along 30° , the system can reach a clogged or partially jammed state. In experimental work, Stoop *et al.*^{38,39} studied the motion of colloidal disks through a random array of obstacles. They found that the flow decreases over time due to the gradual formation of clogged regions.

In this work we examine monodisperse disks moving through a periodic array of obstacles under an external drive that varies in direction from 0° to 90° from the x axis. For low disk densities, the disks flow for every direction of applied drive; however, the net velocity drops at incommensurate angles and reaches a maximum for drives along the easy flow directions of 0° , 45° and 90° . When the disk density is increased, we find that although flow still occurs for driving near 0° and 90° , the system begins to clog at the intermediate angles by forming a phase separated state containing regions of high and low disk density. The clogged system is fragile in nature⁴⁰, and we find a partial hysteresis effect in which the flow can resume if the driving angle is changed after the clogged state forms. We map the locations of the clogged states as a function of obstacle size, and show that there is a critical obstacle size above which even single disks become clogged for driving along the incommensurate directions. We find that a clogged state can undergo a depinning transition to a flowing state if the driving force is increased. Just above the depinning transition, the flow is strongly intermittent and there is a coexistence of clogged states and moving states; however, the moving disks do not exchange neighbors, indicating that the depinning transition is elastic⁴¹. We find that the clogged states are fairly robust to dilution of the obstacle lattice as long as large scale system-spanning dense clusters can still occur; however, when the dilution becomes too strong, the system flows instead of clogging.

Experimental systems in which our results could be tested include particle flow through periodic obstacle arrays^{42–47} or optical trap arrays^{48–52}. Most previous works in such systems were performed in the low density regime where particle-particle interactions are weak. Clogging behavior is expected to occur for high particle densities or in regimes where the diameter of the obstacles is large.

0.1 Simulation

We model a two dimensional $L \times L$ system containing a square array of obstacles with lattice spacing a and obstacle radius r_{obs} . We fix $L = 36$ and $a = 4.0$. Within the system we place N_d mobile disks with dynamics given by the following overdamped equation of motion:

$$\alpha_d \mathbf{v}_i = \mathbf{F}_i^{dd} + \mathbf{F}_i^{\text{obs}} + \mathbf{F}_i^D. \quad (1)$$

The velocity of disk i is $\mathbf{v}_i = d\mathbf{r}_i/dt$, the disk position is \mathbf{r}_i , and the damping constant α_d is set to $\alpha_d = 1.0$. The disk-disk interaction force \mathbf{F}_i^{dd} arises from a harmonic repulsive potential with radius r_d , which we fix to $r_d = 0.5$. The disk-obstacle force $\mathbf{F}_i^{\text{obs}}$ is also modeled with a repulsive harmonic potential. The system density is defined as the total area covered by the obstacles and mobile

disks, $\phi = N_{\text{obs}}\pi r_{\text{obs}}^2/L^2 + N_d\pi r_d^2/L^2$, where N_{obs} is the number of obstacles. The external drive $\mathbf{F}_D = F_D[\cos(\theta)\hat{\mathbf{x}} + \sin(\theta)\hat{\mathbf{y}}]$ is initially applied along the x -direction and gradually rotates from $\theta = 0^\circ$ to $\theta = 90^\circ$ or higher. We measure the average velocity of the disks in the x -direction, $\langle V_x \rangle = \langle \sum_{i=1}^{N_d} \mathbf{v}_i \cdot \hat{\mathbf{x}} \rangle$, where the average is taken over time, and in the y -direction, $\langle V_y \rangle = \langle \sum_{i=1}^{N_d} \mathbf{v}_i \cdot \hat{\mathbf{y}} \rangle$, as well as the net velocity $\langle V \rangle = \sqrt{\langle V_x \rangle^2 + \langle V_y \rangle^2}$. We find that the dynamics can depend on the rate at which the drive direction is changed, so we consider the limit where the direction is changed slowly enough that such effects are absent, which for our parameters is $\delta\theta = 0.000125$ applied every 25000 simulation time steps. In previous work we examined lower disk densities where the system is in the flowing state and exhibits a series of directional locking effects where the disks preferentially flow along specific symmetry directions of the obstacle lattice⁵³. Here we focus on large obstacle sizes and/or large disk densities where clogging effects appear.

0.2 Directional Clogging and Memory Effect

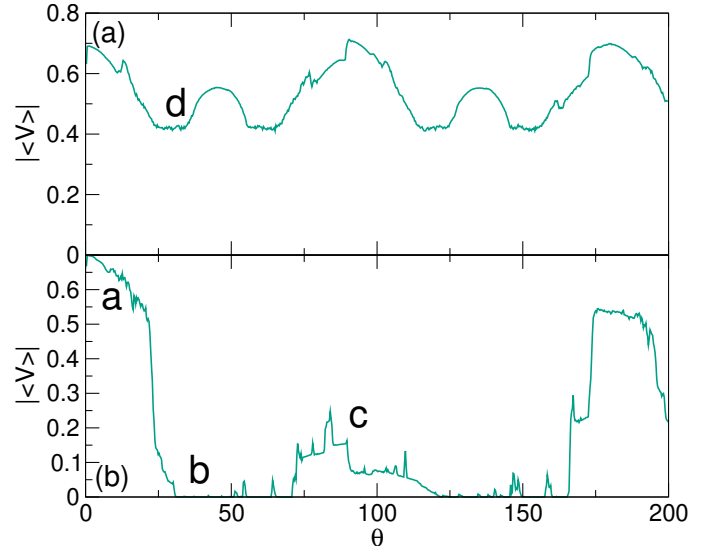


Fig. 1 The instantaneous value of the total velocity $|\langle V \rangle|$ versus driving direction θ for mobile disks moving through a square obstacle array with $r_{\text{obs}} = 1.485$ at $F_D = 0.0025$. (a) At a total system density of $\phi = 0.632$, the disks are always flowing but $|\langle V \rangle|$ has local maxima at $\theta = 0^\circ$, 45° and 90° . (b) At $\phi = 0.68$, there are extended regions where the system is in a clogged state. The labels (a,b,c,d) indicate the values of θ at which the images in Fig. 2 were obtained.

We first consider a system with $r_{\text{obs}} = 1.485$ at $F_D = 0.0025$. In Fig. 1(a) we plot $|\langle V \rangle|$ versus θ at $\phi = 0.632$ where there are $N_{\text{obs}} = 81$ obstacles and $N_d = 330$ mobile disks. If the disks were flowing freely without contacting the obstacles or other disks, we would obtain $|\langle V \rangle| = 0.825$. Figure 1(a) shows that $|\langle V \rangle|$ is finite for all driving angles, indicating that the system is never in a clogged state; however, maxima in $|\langle V \rangle|$ appear at $\theta = 0^\circ$, 45° , and 90° . At these symmetry directions of the substrate array, the disks can minimize the number of collisions that occur with the obstacles, as studied previously⁵³. We find a maximum value of $|\langle V \rangle| \approx 0.7$, corresponding to approximately 85% of the free

disk velocity. In Fig. 1(b), we plot $|\langle V \rangle|$ versus θ for the same system with a larger number $N_d = 409$ of mobile disks, giving $\phi = 0.68$. There are now extended regions of $|\langle V \rangle| = 0.0$ in which the system is in a clogged state, such as for $30^\circ < \theta < 70^\circ$ and $120^\circ < \theta < 167^\circ$. Here the disks are still able to flow along the 0° and 90° symmetry directions of the obstacle array but become clogged for other driving directions. The velocity $|\langle V \rangle| \approx 0.7$ for $\theta = 0^\circ$, is only $|\langle V \rangle| \approx 0.15$ at $\theta = 90^\circ$, and reaches $|\langle V \rangle| \approx 0.54$ for $\theta = 180^\circ$. Thus the magnitude of the velocity has a similar value for driving in the positive or negative x direction but is considerably smaller for driving in the y direction. This hysteresis or memory of the initial driving direction results from the fragility of the clogged states. When the system first enters a clogged phase at $\theta = 30^\circ$, it becomes locked to a configuration that blocks flow for driving along or close to that particular value of θ . When θ increases to 90° , a portion of the configuration remains clogged so the flow is reduced compared to its original positive x direction value. As θ increases to $\theta = 180^\circ$, along the negative x direction, the drive exerts reversed forces on the configurations that formed to block the $\theta = 30^\circ$ flow, destroying these configurations and unclogging the system. When we continue to cycle the value of θ , we always find greater flow along the $\pm x$ directions than along the $\pm y$ directions. If we instead start the system with $\theta = 90^\circ$ so that the flow is along the y direction, we find the opposite effect in which the flow is always higher along the $\pm y$ directions than along the $\pm x$ directions. This indicates that the flow retains a memory of the initial driving direction. For $\phi = 0.632$ in Fig. 1(a), $|\langle V \rangle|$ exhibits little or no memory effect since no clogging occurs, so the values of $|\langle V \rangle|$ at $\theta = 0^\circ$ and $\theta = 90^\circ$ are nearly identical.

In Fig. 2(a) we show a snapshot of the disk and obstacle locations for the system in Fig. 1(b) at $\theta = 2^\circ$ where the disks are flowing along the x direction. Figure 2(b) illustrates the clogged configuration at $\theta = 35^\circ$ where all the disks are immobile and have formed high density regions coexisting with regions that contain no mobile disks. In Fig. 2(c) at $\theta = 90^\circ$, clogged configurations coexist with moving disks which are aligned with the y direction and flowing in the driving direction near the center of the sample. Figure 2(d) shows the obstacle and disk configurations at $\theta = 35^\circ$ for the system in Fig. 1(a) where no clogged state appears and the disk density remains uniform.

As ϕ decreases, the clogging memory effect diminishes, as shown in the plot of $|\langle V \rangle|$ versus θ in Fig. 3(a) for a sample with $\phi = 0.656$. There are two clogged windows, but in the moving regimes, the velocity is nearly equal in magnitude for both $\theta = 0^\circ$ and $\theta = 90^\circ$. In Fig. 3(b) we plot the corresponding velocity components $\langle V_x \rangle$ and $\langle V_y \rangle$ versus θ . When $\theta < 30^\circ$, the flow is predominantly along the x direction, but there is a small amount of motion in the y direction produced by the disk rearrangements that occur as the system enters the clogged state. Both velocity components are zero in the clogged regime. For $70^\circ < \theta < 120^\circ$, the flow is almost exclusively along the y direction since the clogged state formed for driving along the x direction, causing motion along x to be suppressed. The memory effect continues to diminish with decreasing ϕ as shown in Fig. 4 where we plot $\langle V \rangle$ versus ϕ at $\theta = 0^\circ$ and $\theta = 90^\circ$. When the system retains a memory of the driving direction, the net velocity for these two driving directions

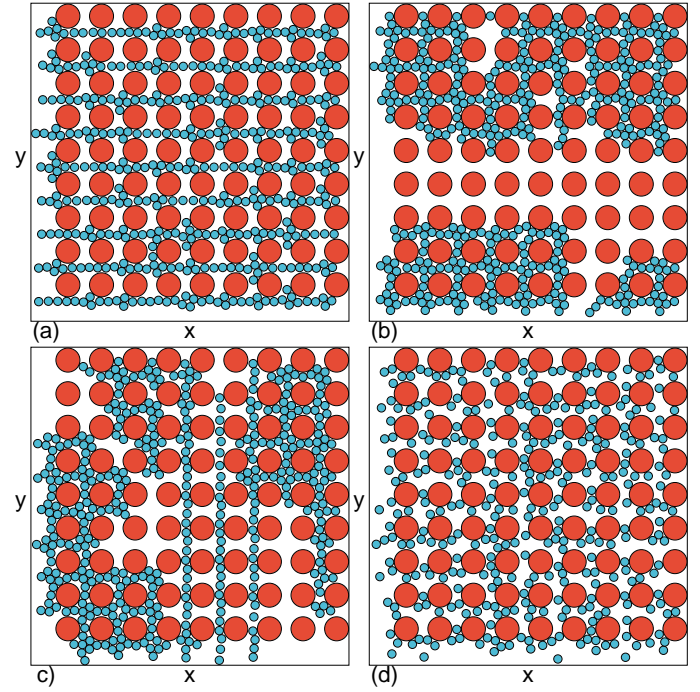


Fig. 2 The obstacle locations (red circles) and mobile disks (blue circles) for the system in Fig. 1(b) with $r_{\text{obs}} = 1.485$, $F_D = 0.0025$, and $\phi = 0.68$ at (a) $\theta = 2^\circ$ where the disks are flowing along the x direction, (b) $\theta = 35^\circ$ where the system is in a clogged state, and (c) $\theta = 90^\circ$ where there is a combination of clogged and flowing disks. (d) The same for the system in Fig. 1(a) with $\phi = 0.632$ at $\theta = 35^\circ$ where a clogged state does not occur.

is different. When $\phi < 0.644$, clogging becomes impossible and the memory effect disappears.

The ability of the system to clog at a fixed mobile disk radius is determined by the driving direction θ , the total density ϕ , and the obstacle radius r_{obs} . The directional dependence arises from the changes in the effective distance a_{eff} between obstacles along the path of the mobile disks. For $\theta = 0^\circ$ and $\theta = 90^\circ$, a_{eff} reaches its maximum value of $a_{\text{eff}} = a$, while at incommensurate angles, a_{eff} is reduced, permitting more frequent collisions between the mobile disks and the obstacles. In Fig. 5 we plot a dynamical phase diagram as a function of θ versus ϕ for the system in Fig. 1 highlighting where the heterogeneous clogged state appears. For $\phi < 0.63$, the system never clogs, while as ϕ increases above $\phi = 0.63$, the width of the clogging phase increases. For $\phi > 0.71$ our initialization procedure cannot pack any more disks into the system; however, we expect that for high disk densities the width of the clogged state would continue to grow until the system becomes jammed for all directions of motion. The formation of a jammed rather than a clogged state would also be associated with the loss of the memory effect since the velocity would be zero for every direction of drive. The nature of the change from clogging to jamming behavior is beyond the scope of the present study. The fragility that we observe in the clogged phase is consistent with the ideas of fragility proposed for certain types of soft matter systems under constraints, where special configurations or force chains must form to block the flow in certain directions⁴⁰.

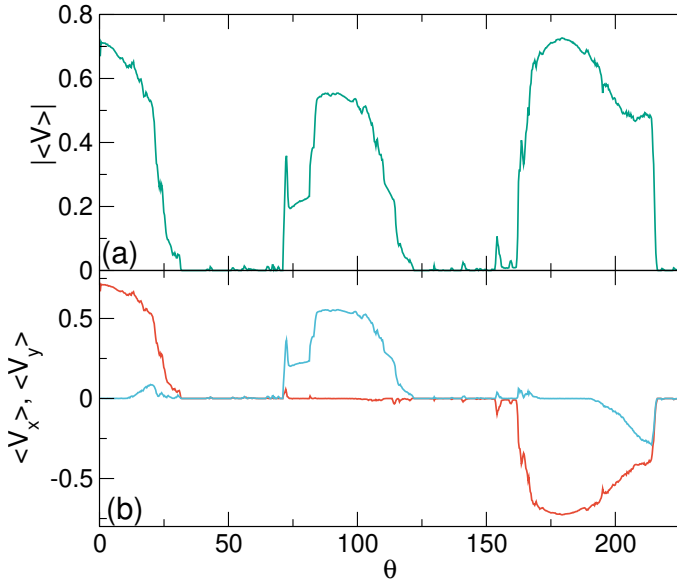


Fig. 3 (a) $\langle |V| \rangle$ vs θ for the system in Fig. 1 with $r_{\text{obs}} = 1.485$ and $F_D = 0.0025$ at a low $\phi = 0.656$ showing two clogged regimes and a reduction of the memory, as indicated by the fact that the velocity is nearly the same for $\theta = 0^\circ$ and $\theta = 90^\circ$. (b) The individual velocity components $\langle V_x \rangle$ (red) and $\langle V_y \rangle$ (blue) vs θ showing that the flow in the non-clogged regions occurs preferentially along the x or y directions.

1 Clogging for Varied Obstacle Size

In Fig. 6(a) we plot the instantaneous disk velocity $|V|$ versus time in simulation time steps for the system in Fig. 1(b) at a fixed drive direction of $\theta = 31^\circ$ with varied obstacle sizes of $r_{\text{obs}} = 1.51, 1.5025, 1.5, 1.495, 1.485, 1.48, \text{ and } 1.475$. The time needed for the system to reach a zero velocity clogged state increases with decreasing r_{obs} . We find two distinct clogging regimes as a function of r_{obs} for this obstacle density. When $r_{\text{obs}} > 1.502$, the spacing between adjacent obstacles is so small that even a single disk can become trapped when attempting to move between the obstacles. The obstacle lattice constant is $a = 4.0$ and the mobile disks have radius $r_d = 0.5$, so there is only exactly enough room for the mobile disk to pass between the obstacles without touching them when $r_{\text{obs}} = 1.5$. Since the disk-obstacle interaction is represented by a very stiff spring rather than a hard wall, disks can still slip between the obstacles even when $r_{\text{obs}} > 1.5$. For $r_{\text{obs}} > 1.5025$, the clogging occurs at the single disk level and is uniform in nature, while for $1.5025 < r_{\text{obs}} < 1.475$, multiple mobile disks must interact in order to form a clogged state, resulting in spatial heterogeneity. For $r_{\text{obs}} < 1.475$, the system is in a flowing state. In the heterogeneous clogging regime, the system remains in its initial flowing state for some time before a collision between mobile disks nucleates a high density clogged region that can spread across the sample, blocking the flow.

In Fig. 7 we illustrate some representative configurations for the system in Fig. 6. Figure 7(a) shows a uniformly clogged state at $r_{\text{obs}} = 1.51$, where the disks are all immobile but the density is uniform. At $r_{\text{obs}} = 1.5025$ in Fig. 7(b), there is a transition to heterogeneous clogging. In Fig. 6(c) we show a heterogeneous clogged state at $r_{\text{obs}} = 1.5$, while at $r_{\text{obs}} = 1.45$ in Fig. 6(d), the

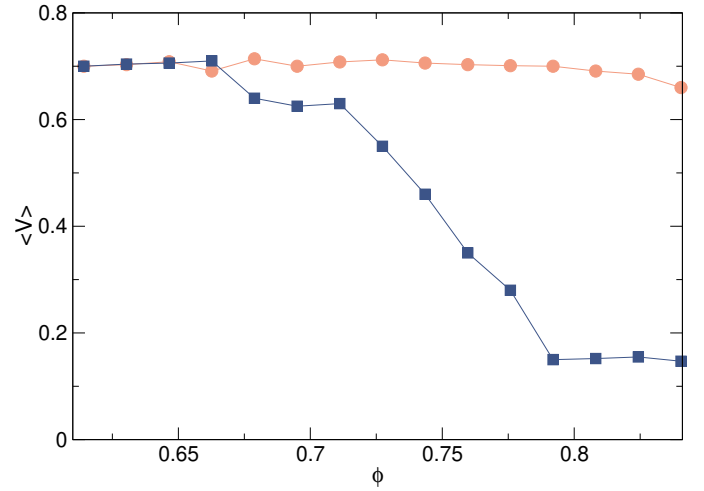


Fig. 4 $\langle V \rangle$ versus density ϕ for the system in Fig. 1 with $r_{\text{obs}} = 1.485$ and $F_D = 0.0025$ at $\theta = 0^\circ$ (orange circles) and $\theta = 90^\circ$ (blue squares). A memory effect in which the velocity at the two values of θ is different appears when $\phi > 0.644$.

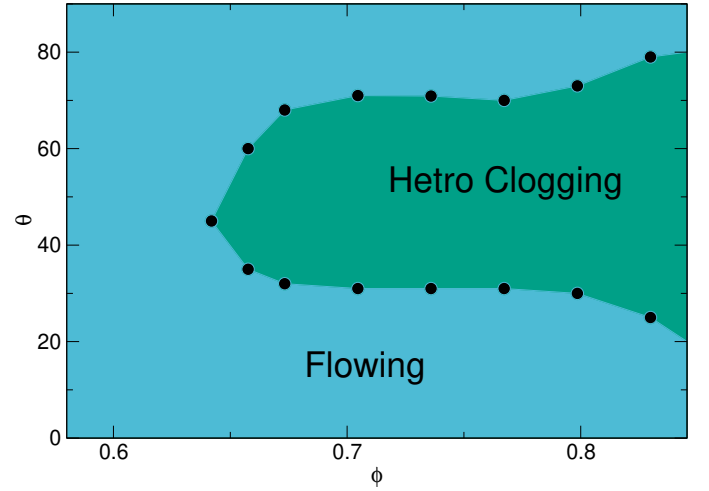


Fig. 5 Dynamical phase diagram as a function of θ versus ϕ for the system in Fig. 1 with $r_{\text{obs}} = 1.485$ and $F_D = 0.0025$ showing the heterogeneous clogging regime (green) and the flowing regime (blue).

disks are flowing.

We measure the time τ required for the system to reach a clogged state by fitting the curves in Fig. 6(a) to the form $|V|(t) \propto \exp(-t/\tau) + V_0$. In Fig. 6(b) we plot τ versus r_{obs} , showing a divergence near a critical obstacle radius of $r_c = 1.4752$. The solid line is a fit to $\tau \propto (r_{\text{obs}} - r_c)^\gamma$ with $\gamma = -1.25$. When $r_{\text{obs}} > 1.5025$, τ drops to a small value since no plastic rearrangements are required for the system to reach a uniform clogged state. The dashed line indicates the transition from the heterogeneous to the uniform clogging behavior. The power law divergence in τ near r_c resembles the time divergence found at reversible to irreversible transitions in periodically sheared colloidal systems^{54,55}, amorphous solids⁵⁶, and superconducting vortices⁵⁷. In previous numerical work on clogging in two-dimensional random obstacle arrays³⁷, a similar power law time divergence with an exponent of $\gamma = -1.29$ appeared when the system entered the clogged phase

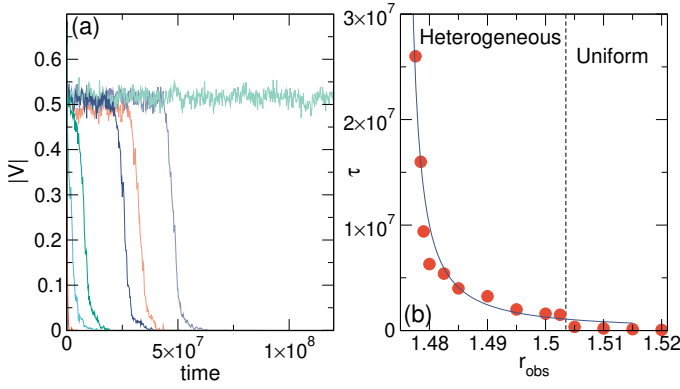


Fig. 6 (a) Instantaneous velocity $|V|$ versus time in simulation time steps for the system in Fig. 1 with $F_D = 0.0025$ and fixed driving angle $\theta = 31^\circ$ for obstacle radius $r_{\text{obs}} = 1.51$ (dark orange), 1.5025 (light blue), 1.5 (dark green), 1.495 (dark blue), 1.485 (light orange), 1.48 (light purple), and 1.475 (light green). (b) The time τ for the system to reach a clogged state vs r_{obs} . The solid line is a fit to $\tau \propto (r_{\text{obs}} - r_c)^{-1.25}$. The dashed line separates the heterogeneous clogging state from the uniform clogged state.

as the obstacle density was varied. These exponents are close to the value expected for an absorbing phase transition, where the clogged state can be viewed as the absorbed state since in this state all fluctuations are lost⁵⁸.

When the obstacles are in a periodic array, the nature of the clogged state depends on the driving direction. For $\theta = 0^\circ$ or $\theta = 90^\circ$, there is only a uniform clogged state for $r_{\text{obs}} > 1.5025$ but there are no heterogeneous clogged states, so we find no power law divergence in the clogging time for these driving directions. At incommensurate angles, the system has a closer resemblance to a random obstacle array, making it possible for a heterogeneous clogged state to appear that is associated with a power law divergence in the time required for the clogged state to organize. In this work we focus only on monodisperse mobile disks, but if the mobile disk radii were bidisperse or multidisperse, the system could exhibit heterogeneous clogging for x and y -direction driving. In this case, the clogging transition would likely shift to lower values of ϕ and r_{obs} .

In Fig. 8 we plot a dynamical phase diagram as a function of r_{obs} versus ϕ for the system in Figs. 6 and 7 where the drive is applied at $\theta = 31^\circ$. For $r_{\text{obs}} > 1.503$, the system forms a uniform clogged state that is independent of ϕ , and the clogged state forms immediately with no diverging time scale. When $\phi > 0.6$ and $1.475 < r_{\text{obs}} < 1.5032$, we find heterogeneous clogging with a power law time divergence for the formation of the clogged state. Similar phase diagrams can be constructed for other driving angles. For example, at $\theta = 0^\circ$ the heterogeneous clogged phase is absent for the same range of system parameters shown in Fig. 8.

In our studies we have not considered the effect of temperature or other perturbations such as activity^{59,60}. Such perturbations are likely to wash out the clogged state due to its fragile nature; however, there could still be some remnant of nonlinear behavior or intermittent dynamics in regions where heterogeneous clogging would occur in the absence of the perturbations.

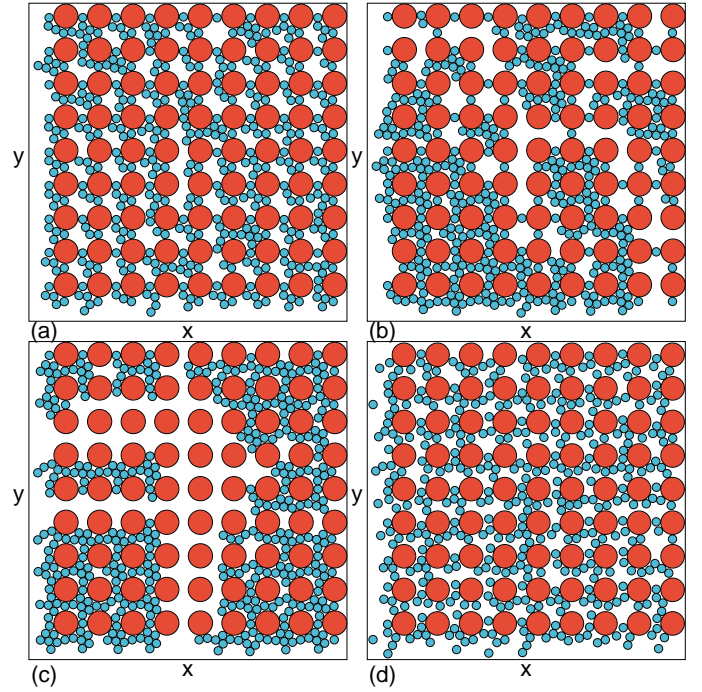


Fig. 7 The obstacle locations (red circles) and mobile disks (blue circles) for the system in Fig. 6 with $F_D = 0.0025$ and $\theta = 31^\circ$. (a) A uniform or homogeneous clogged state at $r_{\text{obs}} = 1.51$. (b) A clogged state for $r_{\text{obs}} = 1.5025$ at the crossover from uniform to heterogeneous clogging. (c) A heterogeneous clogged state at $r_{\text{obs}} = 1.5$. (d) A flowing state at $r_{\text{obs}} = 1.45$.

2 Depinning of the Clogged Phase

Since the disk-disk interactions in our system have a harmonic form, the clogged phase should exhibit a drive dependence or a critical driving force above which it should unclog or depin. This type of depinning or unclogging effect is applicable to systems such as bubbles, emulsions, soft colloids, or magnetic bubbles. On the other hand, in granular matter or other systems with hard core particle-particle interactions where the particles cannot deform easily, such depinning would likely occur only for much stronger drives and would be difficult to access experimentally.

In the previous sections, we considered a drive force of $F_D = 0.0025$ which is well below the depinning threshold. We now sweep the value of F_D to explore the depinning behavior. In Fig. 9 we plot $\langle V \rangle$ versus F_D for the system in Fig. 1 at $\phi = 0.68$ and a drive angle of $\theta = 33.8^\circ$ for $r_{\text{obs}} = 1.525$, 1.51 , 1.5 , 1.49 , and 1.475 . When $r_{\text{obs}} > 1.475$, there is a finite depinning threshold F_c which increases with increasing r_{obs} . At $r_{\text{obs}} = 1.525$, the velocity-force curve has an upward concavity and can be fit to the form $V = (F_D - F_c)^\beta$ with $\beta = 0.44$, as shown in the left side of Fig. 10. In general, systems that exhibit elastic depinning have a depinning exponent of $\beta < 1.0$ ⁴¹. During the depinning process from the clogged state, the disks maintain the same neighbors and there is no plastic flow. At higher drives, the velocity crosses over to a linear form with $V \propto F_D$, as shown in the right side of Fig. 10 which illustrates a fit with $\beta = 0.97$. We generally find that depinning in the uniform clogging phase is elastic, and that the disk density remains uniform in both the pinned and flowing states.

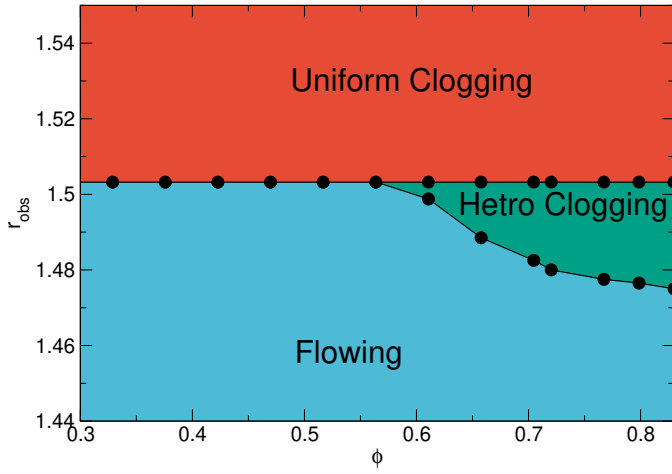


Fig. 8 Dynamical phase diagram as a function of r_{obs} vs ϕ for the system in Fig. 6 with $F_D = 0.0025$ and fixed driving angle $\theta = 31^\circ$ showing the heterogeneous clogging regime (green), flowing regime (blue), and uniform clogging regime (red).

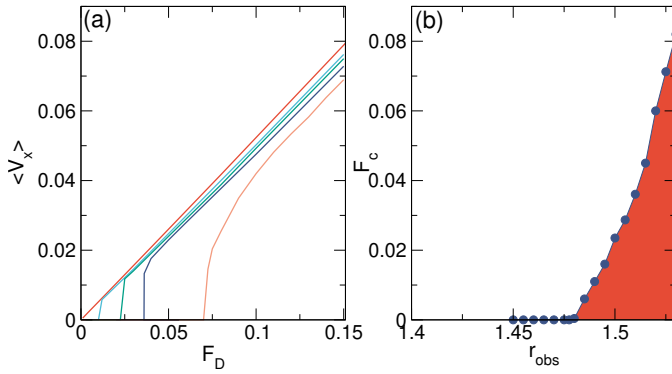


Fig. 9 (a) The average velocity $\langle V \rangle$ vs F_D for the system in Fig. 1 with $\phi = 0.68$ and a drive angle of $\theta = 33.8^\circ$ for $r_{\text{obs}} = 1.525$ (orange), 1.51 (dark blue), 1.5 (green), 1.49 (light blue), and 1.475 (orange red). (b) The depinning threshold F_c vs r_{obs} for the system in (a).

Depinning in the heterogeneous clogged phase is more consistent with a discontinuous jump, which could be indicative of a first order type of transition. Here the pinned state is phase separated but the flowing state has a uniform disk density. This result is consistent with work on the depinning of two-dimensional phase separated systems which has a first order character, both when the pinned state is phase separated and the flowing state is uniform or when the pinned state is uniform and the flowing state is phase separated^{61,62}. In Fig. 9(b) we plot the depinning threshold F_c versus r_{obs} for the system in Fig. 9(a), showing that there is no depinning threshold when $r_{\text{obs}} < 1.475$.

2.1 Fluctuations

We next address the nature of the fluctuations of the flow above the declogging force F_c . Generally we observe highly intermittent flow immediately above the declogging or depinning transition, where regions which are temporarily clogged coexist with moving or flowing regions, while at higher drives all of the disks are flowing. In Fig. 11(a) we plot the instantaneous velocity V ver-

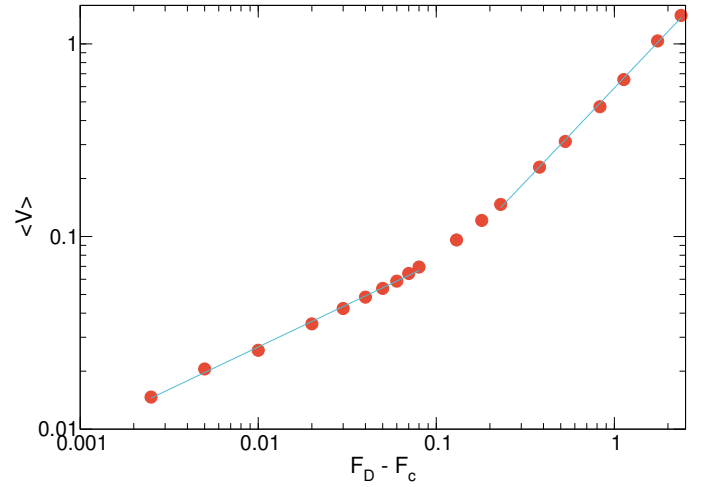


Fig. 10 The scaling of the velocity-force curve from Fig. 9(a) plotted as $\langle V \rangle$ vs $F_D - F_c$ in the uniform clogged phase at $r_{\text{obs}} = 1.525$, where $F_c = 0.07$. Here $\phi = 0.68$ and $\theta = 33.8^\circ$. The leftmost solid line is a power law fit with $\beta = 0.44$, while at higher drives, there is a crossover to a linear behavior with $\beta = 0.97$, as indicated by the rightmost solid line.

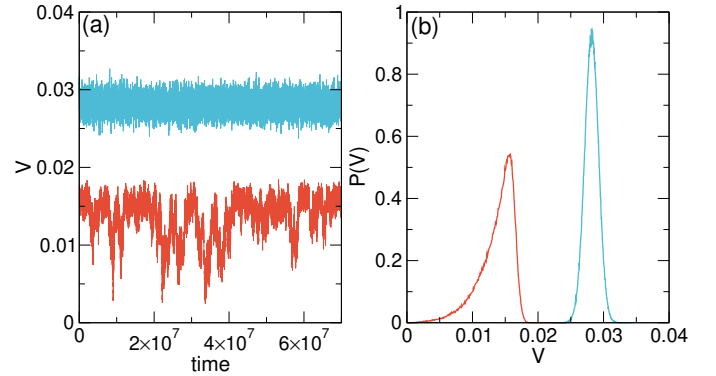


Fig. 11 (a) Instantaneous velocity V vs time in simulation time steps for the system in Fig. 9(a) with $\phi = 0.68$, $\theta = 33.8^\circ$, and $r_{\text{obs}} = 1.51$ at $F_D/F_c = 1.0034$ (red) and $F_D/F_c = 1.67$ (blue). (b) The corresponding velocity distributions $P(V)$.

sus time for the system in Fig. 9(a) with $r_{\text{obs}} = 1.51$ in the uniform clogged phase for $F_D/F_c = 1.0034$, just above the depinning threshold, as well as for a higher drive of $F_D/F_c = 1.67$. There are strong fluctuations in V just above the depinning threshold, while at the higher drive the velocity variations are reduced. The fluctuations near the depinning threshold are strongly non-Gaussian, as shown in Fig. 11(b) where we plot $P(V)$ for the samples in Fig. 11(a). For $F_D/F_c = 1.0034$, $P(V)$ has an enhanced tail at lower drives, producing a strongly skewed distribution, while for $F_D/F_c = 1.67$, $P(V)$ has a more symmetrical Gaussian shape. We observe similar trends for the other values of r_{obs} .

Differences in the noise fluctuations can also be detected by computing the power spectrum of the velocity time series, $S(\omega) = |\int \exp(-2\pi i \omega t) V(t) dt|^2$. In Fig. 12 we plot $S(\omega)$ for the system in Fig. 11(a). For $F_D/F_c = 1.0034$, the fluctuations have a $1/f^\alpha$ or broad band noise character with $\alpha = -1.5$, while for $F_D/F_c = 1.67$, we find a white noise signature with $\alpha = 0$. There are peaks in $S(\omega)$ at higher ω produced by the periodic signal from the disks

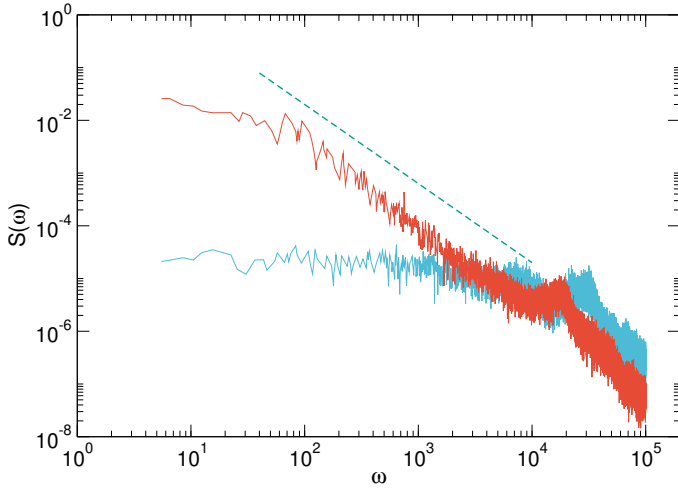


Fig. 12 The power spectra $S(\omega)$ vs ω for the system in Fig. 11(a) with $\phi = 0.68$, $\theta = 33.8^\circ$, and $r_{\text{obs}} = 1.51$ at $F_D/F_C = 1.0034$ (red) and $F_D/F_C = 1.67$. The dashed line is a power law fit of the $F_D/F_C = 1.0034$ curve to $\alpha = -1.5$, while the $F_D/F_C = 1.67$ curve exhibits white noise at lower frequencies with $\alpha = 0$.

encountering the obstacle lattice. The lower frequency $1/f^\alpha$ noise is associated with long time large scale changes in the disk configurations. Even under very strong fluctuations, the velocity above the depinning transition never drops to zero because this would cause the system to be permanently captured in a clogged state. In contrast, other systems with constant flux or some periodic perturbation would show intermittent flow that would be expected to have $1/f^\alpha$ noise characteristics. Studies of clogging in bottlenecks have also found strongly intermittent dynamics including power law distributions of bursts^{63,64}.

3 Clogging in Diluted Arrays

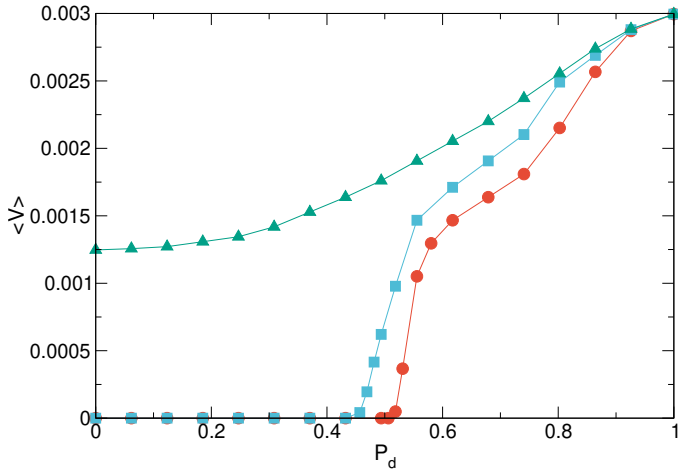


Fig. 13 The net velocity $\langle V \rangle$ vs the dilution factor P_d for random dilution of the square array in the system from Fig. 9 with an undiluted value of $\phi = 0.68$, $\theta = 33.8^\circ$ and $F_D = 0.0029$ at $r_{\text{obs}} = 1.525$ (red circles), 1.485 (blue squares), and 1.475 (green triangles).

In the absence of obstacles, the disks would flow for any finite drive. Thus we study random dilution of the obstacle array in order to observe the transition from a clogged state to a flowing

phase. We select a fraction P_d of obstacles to remove at random from the system in Fig. 9 with an undiluted value of $\phi = 0.68$, $\theta = 33.8^\circ$, and $F_D = 0.0029$, well below the depinning threshold of the undiluted sample. In Fig. 13 we plot $\langle V \rangle$ versus the dilution fraction P_d for $r_{\text{obs}} = 1.525$, $r_{\text{obs}} = 1.485$, and $r_{\text{obs}} = 1.475$. The $r_{\text{obs}} = 1.475$ has no depinning threshold even when $P_d = 0$, and as P_d increases, there is a gradual increase in $\langle V \rangle$ which reaches a saturation value of F_D near $F_D = 1.0$. In the $r_{\text{obs}} = 1.525$ sample, the depinning threshold for $P_d = 0$ is $F_C = 0.07$. As P_d increases, the system remains clogged up to $P_d = 0.52$, and then there is a gradual increase in $\langle V \rangle$ as the dilution fraction becomes larger. In general, we find that when the $P_d = 0$ depinning threshold is finite, the dilution needs to be greater than $P_d = 0.44$ in order to unclog the system, as shown for the $r_{\text{obs}} = 1.485$ sample. This indicates that the transition from a clogged to a flowing state is probably related to a percolation transition.

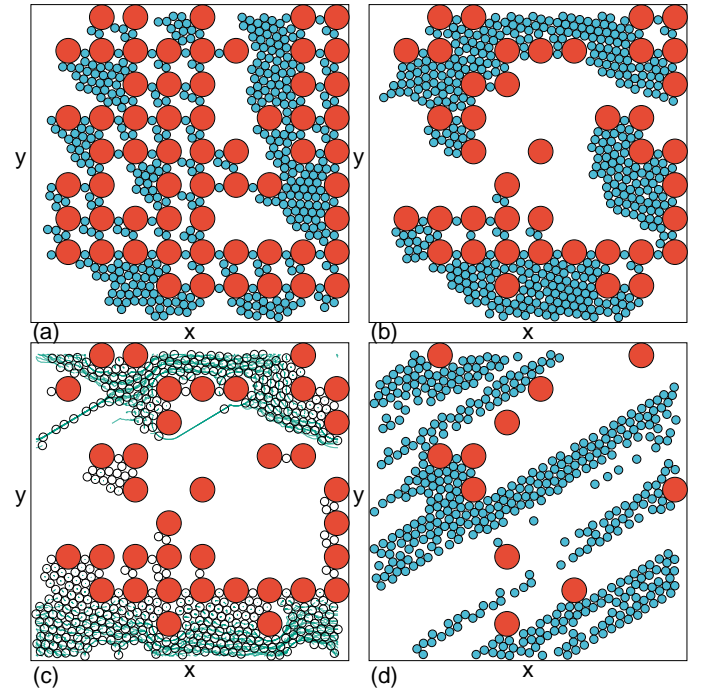


Fig. 14 The obstacle locations (red circles) and mobile disks (blue circles) for the system in Fig. 13 with an undiluted value of $\phi = 0.68$, $F_D = 0.0025$ and $\theta = 31^\circ$ at $r_{\text{obs}} = 1.525$ under different pinning dilutions P_d . (a) The clogged phase at $P_d = 0.25$. (b) The clogged phase at $P_d = 0.494$. (c) The moving phase at $P_d = 0.56$ where green lines indicate the trajectories of the mobile disks. (d) The heterogeneous moving phase at $P_d = 0.86$.

As the dilution is increased, the time required for the system to organize to a steady state increases but shows strong fluctuations if different initializations of the mobile disk locations are used. When $r_{\text{obs}} = 1.525$, the $P_d = 0$ sample forms a uniform clogged state; however, as the dilution increases up to $P_d = 0.5$, the clogged state becomes increasingly heterogeneous. This is illustrated in Fig. 14. At $P_d = 0.25$ in Fig. 14(a), the system is strongly spatially heterogeneous but is still clogged. The clogged state that appears at $P_d = 0.494$ just before the transition to a moving phase is shown in Fig. 14(b). For $0.52 < P_d < 0.62$, clogged regions coexist with moving regions, resulting in plastic flow as

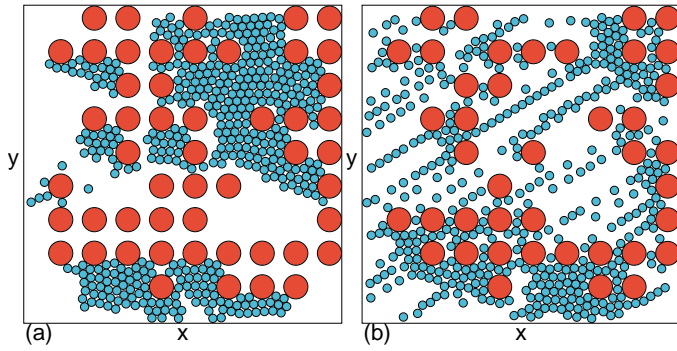


Fig. 15 The obstacle locations (red circles) and mobile disks (blue circles) for the system in Fig. 13 with an undiluted value of $\phi = 0.68$, $F_D = 0.0025$, and $\theta = 31^\circ$. (a) At $r_{\text{obs}} = 1.485$ and $P_d = 0.37$ in a barely clogged state, the disk arrangement is strongly heterogeneous. (b) A flowing state at $r_{\text{obs}} = 1.475$ and $P_d = 0.494$.

indicated in Fig. 14(c) at $P_d = 0.56$. At high dilution, the system forms a moving phase that is distinguished from the moving states found in undiluted arrays by its strong spatial heterogeneity, as shown in Fig. 14(d) for a sample with $P_d = 0.86$. We observe similar dynamics in the diluted systems whenever the depinning threshold is finite. In Fig. 15(a) we plot a barely clogged configuration at $r_{\text{obs}} = 1.485$ and a dilution of $P_d = 0.37$, showing a heterogeneous spanning clogged state, while in Fig. 15(b) we illustrate the moving state at $r_{\text{obs}} = 1.475$ and $P_d = 0.49$, where a few regions are locally clogged but the system remains in a flowing state.

4 Conclusions

We have examined the clogging dynamics for a monodisperse assembly of disks moving through a periodic obstacle array. We find that the susceptibility for the system to clog under fixed disk density and obstacle radius depends on the direction of drive relative to the symmetry of the obstacle lattice. The system clogs at incommensurate driving angles or for angles in the range $30^\circ < \theta < 70^\circ$; however, the range of parameters over which clogging occurs increases with increasing system density and obstacle size. The systems is least susceptible to clogging for drives centered around $\theta = 0^\circ$ and $\theta = 90^\circ$. Under a changing drive angle the system exhibits a memory effect in which the formation of a clogged state for one driving direction results in a reduced flow rate when the drive is rotated into the perpendicular direction. The memory effect is lost as the disk density or obstacle radius decreases. We observe two distinct types of clogging states: heterogeneous or phase separated clogging in which groups of disks must gradually arrange themselves into a clogged configuration, and a uniform clogged state in which the spacing between adjacent obstacles is small enough that individual disks can be trapped immediately. Since we represent the disk-disk interactions with a stiff harmonic potential, a clogged state can be unclogged by increasing the driving force and inducing a depinning transition. The disk configurations are generally uniform in the unpinned phase. For drives just above the unclogging transition, the velocity exhibits strong non-Gaussian fluctuations with a $1/f^\alpha$ noise characteristic, where $\alpha \approx 1.5$. At higher drives, the velocity distribution

becomes Gaussian and the fluctuations have a white noise signature. We also show that a clogged to unclogged transition can be produced when the obstacle lattice is diluted through the random removal of a fraction of obstacles. The disk arrangement becomes increasingly heterogeneous for increasing dilution, and a transition to an unclogged state occurs for dilution fractions close to 0.5, indicating that the transition has a percolative character. Our results should be relevant for clogging dynamics in soft colloidal systems, emulsions, and bubbles. Similar clogging effects could also occur for magnetic bubbles, skyrmions, or superconducting vortices moving through periodic pinning or obstacle arrays.

Conflicts of interest

There are no conflicts to declare.

Acknowledgements

This work was supported by the US Department of Energy through the Los Alamos National Laboratory. Los Alamos National Laboratory is operated by Triad National Security, LLC, for the National Nuclear Security Administration of the U. S. Department of Energy (Contract No. 892333218NCA000001).

Notes and references

- 1 A. J. Liu and S. R. Nagel, *Nature (London)*, 1998, **396**, 21–22.
- 2 C. S. O’Hern, L. E. Silbert, A. J. Liu and S. R. Nagel, *Phys. Rev. E*, 2003, **68**, 011306.
- 3 J. A. Drocco, M. B. Hastings, C. J. O. Reichhardt and C. Reichhardt, *Phys. Rev. Lett.*, 2005, **95**, 088001.
- 4 A. J. Liu and S. R. Nagel, *Annual Review of Condensed Matter Physics*, 2010, **1**, 347–369.
- 5 C. Reichhardt and C. J. O. Reichhardt, *Soft Matter*, 2014, **10**, 2932–2944.
- 6 P. Olsson and S. Teitel, *Phys. Rev. Lett.*, 2007, **99**, 178001.
- 7 L.-N. Zou, X. Cheng, M. L. Rivers, H. M. Jaeger and S. R. Nagel, *Science*, 2009, **326**, 408–410.
- 8 L. M. Lopatina, C. J. Olson Reichhardt and C. Reichhardt, *Phys. Rev. E*, 2011, **84**, 011303.
- 9 R. S. Hoy, *Phys. Rev. Lett.*, 2017, **118**, 068002.
- 10 R. Candelier and O. Dauchot, *Phys. Rev. E*, 2010, **81**, 011304.
- 11 D. Bi, J. Zhang, B. Chakraborty and R. P. Behringer, *Nature (London)*, 2011, **480**, 355–358.
- 12 K. To, P.-Y. Lai and H. K. Pak, *Phys. Rev. Lett.*, 2001, **86**, 71–74.
- 13 C. C. Thomas and D. J. Durian, *Phys. Rev. E*, 2013, **87**, 052201.
- 14 D. Chen, K. W. Desmond and E. R. Weeks, *Soft Matter*, 2012, **8**, 10486–10492.
- 15 I. Zuriguel, D. R. Parisi, R. C. Hidalgo, C. Lozano, A. Janda, P. A. Gago, J. P. Peralta, L. M. Ferrer, L. A. Pugnali, E. Clément, D. Maza, I. Pagonabarraga and A. Garcimartín, *Sci. Rep.*, 2015, **4**, 7324.
- 16 D. Gella, I. Zuriguel and D. Maza, *Phys. Rev. Lett.*, 2018, **121**, 138001.
- 17 C. J. O. Reichhardt and C. Reichhardt, *J. Phys.: Condens. Matt.*, 2018, **30**, 244005.

- 18 S. Redner and S. Datta, *Phys. Rev. Lett.*, 2000, **84**, 6018–6021.
- 19 F. Chevoir, F. Gaulard and N. Roussel, *EPL*, 2007, **79**, 14001.
- 20 N. Roussel, T. L. H. Nguyen and P. Coussot, *Phys. Rev. Lett.*, 2007, **98**, 114502.
- 21 H. M. Wyss, D. L. Blair, J. F. Morris, H. A. Stone and D. A. Weitz, *Phys. Rev. E*, 2006, **74**, 061402.
- 22 C. Barre and J. Talbot, *J. Stat. Mech.*, 2017, **2017**, 043406.
- 23 C. J. Olson Reichhardt, E. Groopman, Z. Nussinov and C. Reichhardt, *Phys. Rev. E*, 2012, **86**, 061301.
- 24 C. Reichhardt and C. J. O. Reichhardt, *Phys. Rev. E*, 2018, **97**, 052613.
- 25 M. Le Blay, M. Adda-Bedia and D. Bartolo, *Proc. Natl. Acad. Sci. (USA)*, 2020, **117**, 13914–13920.
- 26 M. Alava, M. Dubé and M. Rost, *Adv. Phys.*, 2004, **53**, 83–175.
- 27 D. L. Liu, P. R. Johnson and M. Elimelech, *Environ. Sci. Technol.*, 1995, **29**, 2963–2973.
- 28 F. Wirner, C. Scholz and C. Bechinger, *Phys. Rev. E*, 2014, **90**, 013025.
- 29 E. Dressaire and A. Sauret, *Soft Matter*, 2017, **13**, 37–48.
- 30 Q. Liu, B. Zhao and J. C. Santamarina, *J. Geophys. Res.: Solid Earth*, 2019, **124**, 9495–9504.
- 31 G. Gerber, S. Rodts, P. Aïmedieu, P. Faure and P. Coussot, *Phys. Rev. Lett.*, 2018, **120**, 148001.
- 32 G. Gerber, M. Bensouda, D. A. Weitz and P. Coussot, *Phys. Rev. Lett.*, 2019, **123**, 158005.
- 33 C. Brito, G. Parisi and F. Zamponi, *Soft Matter*, 2013, **9**, 8540–8546.
- 34 A. L. Graves, S. Nashed, E. Padgett, C. P. Goodrich, A. J. Liu and J. P. Sethna, *Phys. Rev. Lett.*, 2016, **116**, 235501.
- 35 P. Wentworth-Nice, S. A. Ridout, B. Jenike, A. Liloia and A. L. Graves, *Soft Matter*, 2020, **16**, 5305–5313.
- 36 H. T. Nguyen, C. Reichhardt and C. J. O. Reichhardt, *Phys. Rev. E*, 2017, **95**, 030902.
- 37 H. Peter, A. Libál, C. Reichhardt and C. J. O. Reichhardt, *Sci. Rep.*, 2018, **8**, 10252.
- 38 R. L. Stoop and P. Tierno, *Commun. Phys.*, 2018, **1**, 68.
- 39 S. G. Leyva, R. L. Stoop, P. Tierno and I. Pagonabarraga, *Soft Matter*, 2020, **16**, 6985–6992.
- 40 M. E. Cates, J. P. Wittmer, J.-P. Bouchaud and P. Claudin, *Phys. Rev. Lett.*, 1998, **81**, 1841–1844.
- 41 C. Reichhardt and C. J. O. Reichhardt, *Rep. Prog. Phys.*, 2017, **80**, 026501.
- 42 L. R. Huang, E. C. Cox, R. H. Austin and J. C. Sturm, *Science*, 2004, **304**, 987–990.
- 43 Z. Li and G. Drazer, *Phys. Rev. Lett.*, 2007, **98**, 050602.
- 44 B. R. Long, M. Heller, J. P. Beech, H. Linke, H. Bruus and J. O. Tegenfeldt, *Phys. Rev. E*, 2008, **78**, 046304.
- 45 J. McGrath, M. Jimenez and H. Bridle, *Lab Chip*, 2014, **14**, 4139–4158.
- 46 B. H. Wunsch, J. T. Smith, S. M. Gifford, C. Wang, M. Brink, R. L. Bruce, R. H. Austin, G. Stolovitzky and Y. Astier, *Nature Nanotechnol.*, 2016, **11**, 936–940.
- 47 R. L. Stoop, A. V. Straube, T. H. Johansen and P. Tierno, *Phys. Rev. Lett.*, 2020, **124**, 058002.
- 48 P. T. Korda, M. B. Taylor and D. G. Grier, *Phys. Rev. Lett.*, 2002, **89**, 128301.
- 49 M. P. MacDonald, G. C. Spalding and K. Dholakia, *Nature (London)*, 2003, **426**, 421–424.
- 50 T. Bohlein, J. Mikhael and C. Bechinger, *Nature Mater.*, 2012, **11**, 126–130.
- 51 M. P. N. Juniper, A. V. Straube, D. G. A. L. Aarts and R. P. A. Dullens, *Phys. Rev. E*, 2016, **93**, 012608.
- 52 X. Cao, E. Panizon, A. Vanossi, N. Manini and C. Bechinger, *Nature Phys.*, 2019, **15**, 776.
- 53 C. Reichhardt and C. J. O. Reichhardt, *Phys. Rev. E*, 2020, **102**, 022608.
- 54 L. Corte, P. M. Chaikin, J. P. Gollub and D. J. Pine, *Nature Phys.*, 2008, **4**, 420–424.
- 55 L. Milz and M. Schmiedeberg, *Phys. Rev. E*, 2013, **88**, 062308.
- 56 I. Regev, T. Lookman and C. Reichhardt, *Phys. Rev. E*, 2013, **88**, 062401.
- 57 S. Okuma, Y. Tsugawa and A. Motohashi, *Phys. Rev. B*, 2011, **83**, 012503.
- 58 H. Hinrichsen, *Adv. Phys.*, 2000, **49**, 815–958.
- 59 C. Reichhardt and C. J. O. Reichhardt, *Phys. Rev. Lett.*, 2018, **121**, 068001.
- 60 B. Ai, F. Meng, Y. He and X. Zhang, *Soft Matter*, 2019, **15**, 3443–3450.
- 61 C. Reichhardt, C. J. O. Reichhardt, I. Martin and A. R. Bishop, *Phys. Rev. Lett.*, 2003, **90**, 026401.
- 62 C. Reichhardt, C. J. Olson, I. Martin and A. R. Bishop, *Europhys. Lett.*, 2003, **61**, 221–227.
- 63 D. Gella, I. Zuriguel and J. Ortín, *Phys. Rev. Lett.*, 2019, **123**, 218004.
- 64 M. Souzy, I. Zuriguel and A. Marin, *Phys. Rev. E*, 2020, **101**, 060901.